Materials Today Bio 16 (2022) 100431

Contents lists available at ScienceDirect

Materials Today Bio

journal homepage: www.journals.elsevier.com/materials-today-bio

PVA/pectin composite hydrogels inducing osteogenesis for bone regeneration

Ziwei Hu [a,b,c,d,1], Jianwen Cheng [a,b,c,d,e,1], Sheng Xu [a,b,c,d,f,1], Xiaojing Cheng [a,b,c,d,g,1], Jinmin Zhao [a,b,c,d,e], Zhi Wei Kenny Low [h], Pei Lin Chee [h], Zhenhui Lu [a,b,c,d,*], Li Zheng [a,b,c,d,**], Dan Kai [h,i,***]

[a] Guangxi Engineering Center in Biomedical Material for Tissue and Organ Regeneration, The First Affiliated Hospital of Guangxi Medical University, Nanning, 530021, China
[b] Collaborative Innovation Centre of Regenerative Medicine and Medical BioResource Development and Application Co-constructed By the Province and Ministry, The First Affiliated Hospital of Guangxi Medical University, Nanning, 530021, China
[c] Research Center for Regenerative Medicine, The First Affiliated Hospital of Guangxi Medical University, Nanning, 530021, China
[d] Guangxi Key Laboratory of Regenerative Medicine, The First Affiliated Hospital of Guangxi Medical University, Nanning, 530021, China
[e] Department of Orthopaedics Trauma and Hand Surgery, The First Affiliated Hospital of Guangxi Medical University, Nanning, 530021, China
[f] School of Basic Medical Sciences, Guangxi Medical University, Nanning, 530021, China
[g] Life Science Institute, Guangxi Medical University, Nanning, 530021, China
[h] Institute of Materials Research and Engineering (IMRE), A*STAR, 2 Fusionopolis Way, #08-03 Innovis, 138634, Singapore
[i] Institute of Sustainability for Chemicals, Energy and Environment (ISCE2), A*STAR, 2 Fusionopolis Way, Innovis, #08-03, 138634, Singapore

ARTICLE INFO

Keywords:
Poly (vinyl alcohol)
Pectin
Composite hydrogel
Osteogenesis
Tissue engineering

ABSTRACT

Hydrogels composed from biomolecules have gained great interests as biomaterials for tissue engineering. However, their poor mechanical properties limit their application potential. Here, we synthesized a series of tough composite hydrogels from poly (vinyl alcohol) (PVA) and pectin for bone tissue engineering. With a balance of scaffold stiffness and pore size, PVA-Pec-10 hydrogel enhanced adhesion and proliferation of osteoblasts. The hydrogel significantly promoted osteogenesis *in vitro* by improving the alkaline phosphates (ALP) activity and calcium biomineralization, as well as upregulating the expressions of osteoblastic genes. The composite hydrogel also accelerated the bone healing process *in vivo* after transplantation into the femoral defect. Additionally, our study demonstrated that pectin and its Ca^{2+} crosslinking network play a crucial role of inducing osteogenesis through regulating the Ca^{2+}/CaMKII and BMP-SMAD1/5 signaling. The optimized structure composition and multifunctional properties make PVA-Pec hydrogel highly promising to serve as a candidate for bone tissue regeneration.

1. Introduction

Bone fracture is a common occurrence and affects millions of people worldwide. There are multiple drawbacks related to the repair efficiency of bone defects by traditional therapeutic strategies including allograft and autograft [1]. Donor shortage is one of the main limitations for autograft, while the allograft holds high risk of immunological response and infectious diseases [2]. This probably explains the growing interests in bone tissue engineering, which can circumvent the existing problems of donor shortage and high risk of immunological response. Up to present, various types of materials have been explored for bone regenerative applications, including calcium phosphate ceramics (e.g., hydroxyapatite and β-tricalcium phosphate), bioactive glasses and polymers [3].

Hydrogels are three-dimensional polymeric networks containing a

* Corresponding author. Guangxi Engineering Center in Biomedical Material for Tissue and Organ Regeneration, Guangxi Medical University, Nanning, 530021, China.
** Corresponding author. Guangxi Engineering Center in Biomedical Material for Tissue and Organ Regeneration, Guangxi Medical University, Nanning, 530021, China.
*** Corresponding author. Institute of Materials Research and Engineering (IMRE), A*STAR, 2 Fusionopolis Way, #08-03 Innovis, 138634, Singapore.
E-mail addresses: zhenhuilu1989@163.com (Z. Lu), zhengli224@163.com (L. Zheng), kaid@imre.a-star.edu.sg (D. Kai).
[1] Ziwei Hu, Jianwen Cheng and Sheng Xu contributed as first authors.

https://doi.org/10.1016/j.mtbio.2022.100431
Received 7 April 2022; Received in revised form 31 August 2022; Accepted 13 September 2022
Available online 15 September 2022

huge amount of water (>80%) that exhibit similar structural integrity to native extracellular matrix (ECM) [4,5]. Bestowed with inherent biocompatibility from their high water content, hydrogels are considered one of the most attractive scaffold candidates for bone tissue engineering. Unfortunately, they do not display the desirable fracture toughness and strength that are demanded by the scaffolds used in load bearing applications. To overcome this obstacle, efforts have been devoted to reinforce or strengthen the mechanics of hydrogels, such as the inclusion of inorganic nanoparticles [6], the formulation of nanostructure [7] or the fabrication of composite hydrogels [8]. Among these efforts, composite hydrogels based on two distinct interpenetrating polymer networks emerge as an unique way to reinforce the mechanical properties of the hydrogels [9]. Composite hydrogels that consist of a rigid network and a flexible network can consume the fracture energy effectively during the deformation process and maintain the integrity of the hydrogels simultaneously. The dynamic networks not only elevate the mechanical properties of composite hydrogels, but also endow them with shape memory capability. For example, polyacrylamide (PAAm)/gelatin 3D-printed shape-memory composite hydrogel cross-linked by permanent bonds and dynamic reversible bonds exhibited higher toughness, up to 7 times, in comparison to the hydrogel formed with single network [10]. The reconstruction of the chitosan network based on the dynamic crosslinking points between chitosan chains led to the development of an ultra-high strength composite hydrogel (poly (N-(2-hydroxyethyl) acrylamide)/chitosan-anions) with good fatigue resistance and self-recovery ability [11]. The method has also enabled Mredha et al. to achieve a novel class of collagen fibril-based tough hydrogel termed hydroxyapatite/swim bladder collagen/N, N′-dimethylacrylamide that possessed mechanical properties in the range of the natural cartilage [12].

Poly (vinyl alcohol) (PVA) has attracted immense attention in biomedical applications owing to its inherent advantageous mechanical properties, low cytotoxicity and FDA approval for oral medicine usage [13]. However, its synthetic nature and insufficient cell adhesion remain challenging for its application in bone tissue engineering arena. Pectin, on the other hand, is a natural polysaccharide extracted from the plant cell walls [14,15]. Being biocompatible and biodegradable, it holds great potential to be explored for tissue engineering uses, specifically as scaffold that can serve as artificial ECM. The good gelling properties of pectin provides the ease to design and develop scaffolds [16,17]. As an anionic polysaccharide, pectin undergoes calcium-induced gelation to form the "egg box" like structure to immobilize drugs, proteins and cells within the hydrogels [16,18]. Besides, it was reported that Ca^{2+} and mechanotransduction promote the expression of osteoblast-specific proteins and cell proliferation that are essential for bone regeneration [19]. The binding of Ca^{2+} and calmodulin (CaM), which is a small Ca^{2+}-binding protein and a principal mediator of Ca^{2+} signal in eukaryotic cells, leads to the formation of Ca^{2+}/CaM complex [20]. The complex is responsible for the phosphorylation and the activation of the calmodulin-dependent kinase II (CaMK-II) which in turn plays a crucial role in regulating the functions of osteoblasts [21,22]. Bone morphogenetic 2 (BMP-2) signaling and mechanotransduction pathways are tightly interconnected. The activation of osteogenic genes requires the cooperation of BMP-2 pathway-associated Smad1/5 heteromeric complexes [23].

Herein, we designed and synthesized a tough physical hydrogel system from PVA and pectin (PVA-Pec) targeted for bone tissue engineering. The composite hydrogel was built up based on two networks: the primary network being semicrystalline PVA polymers assembled by cyclic freeze-thawing procedures and the secondary one by the ionic interaction between calcium and pectin. Given the nature of pectin as a polyuronate, the gelation process was facile and reproducible, achievable with the introduction of calcium ions. In addition, the attained "egg-box" structure supports the immobilization of bioactive components or cells inside the gel structure making the system an ideal candidate for tissue engineering application [24]. Through adjustment of the polymer content in the system, the physicochemical and mechanical properties of the biomimetic PVA-Pec hydrogels were assessed and optimized. The optimized hydrogel was then selected for *in vitro* study, to evaluate the cell adhesion, proliferation and mineralization ability. Additionally, the system was further assessed *in vivo* for its applicability in supporting bone healing. The Ca^{2+}/calmodulin (CaM) and BMP-SMAD1/5 signaling that underlying the osteogenic effect of PVA-Pec hydrogel was also investigated.

2. Materials and methods

2.1. Materials

Anhydrous calcium chloride, pectin (galacturonic acid>74.0%), PVA (M_w = 130,000, 99+ % hydrolyzed), dimethyl sulfoxide (DMSO), and 3-(4, 5-dimethylthiazol-2-yl)-2, 5-diphenyltetrazolium bromide (MTT) were purchased from Sigma-Aldrich. Deionized (DI) water (18.2 MΩ) was used in all synthesis and immersion steps. Cetylpyridinium chloride was obtained from Macklin (Shanghai, China). All chemicals used in this experiment were of analytical grade and used without further purification.

2.2. Hydrogel fabrication

The PVA-Pec composite hydrogel was fabricated by the freezing-thawing process. The fabrication process was illustrated in Fig. 1a. PVA and pectin were mixed in a weight ratio of 8:1 and homogeneously distributed in DI water at 95 °C for 2 h. The well-mixed solution was poured into pre-heated moulds and kept in −20 °C for 72 h, followed by room temperature for 1 h. The above freezing-thawing process was repeatedly implemented two more times at freezing time for 23 h and thawing time for 1 h respectively. The mixture was then immersed in calcium chloride solution (5 M) for 24 h followed by in DI water until the gel reached equilibrium swelling. Final samples were defined as PVA-Pec-x, where x represented the total quantities of polymers in the volume of homogenized solution (w/v).

2.3. Scanning electron microscopy (SEM)

Hydrogels in the equilibrium swelling state was dried with supercritical CO_2. Their cross-sections were coated with gold and the morphology was observed by using a scanning electron microscope (SEM; JEOL, Japan).

2.4. Swelling and degradation tests

For swelling characterization, the fabricated hydrogels were lyophilized to obtain their dry weight W_d. These samples were separately immersed in DI water, and their weights were monitored daily until no significant change was observed to obtain the equilibrium swelling weight, W_{eq}. The experiments were performed in triplicate under the same conditions and the equilibrium water content (EWC) was calculated by equation (1):

$$EWC\ (\%) = \frac{w_{eq} - w_d}{w_{eq}} \times 100 \quad (1)$$

For the *in vitro* degradation, lyophilized samples were weighted at initial time (M_0) and incubated in PBS (pH 7.4) at 37 °C. At a predetermined time, samples were lyophilized and the remaining mass (Mt) was measured. The degradation rate of hydrogels was calculated using equation (2).

$$Weight\ loss\ (\%) = \frac{w_0 - w_t}{w_0} \times 100 \quad (2)$$

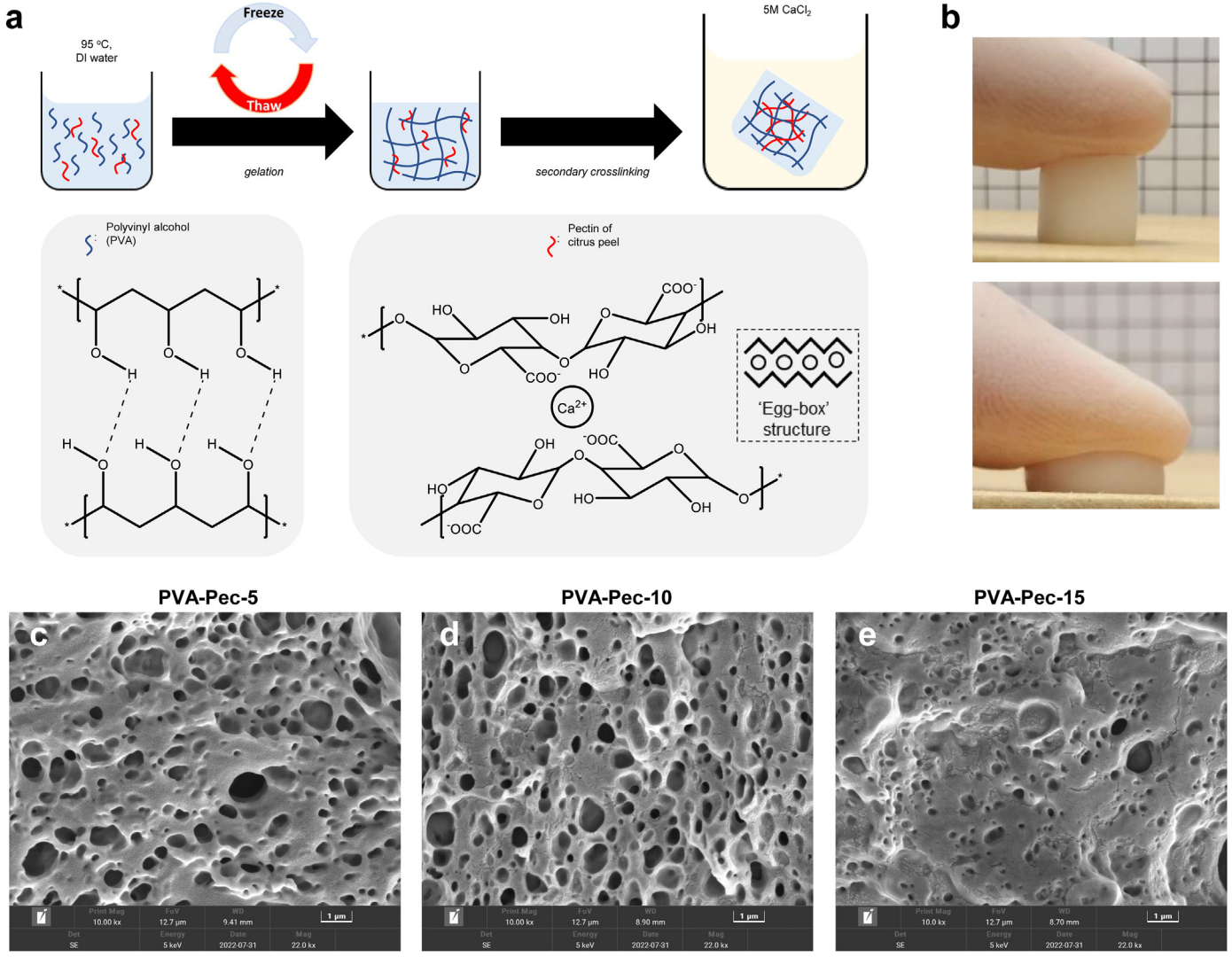

Fig. 1. (**a**) Fabrication process of PVA-Pec hydrogels. (**b**) Compression of PVA-Pec hydrogels with a finger. (**c-e**) SEM images showing cross-sections of (**c**) PVA-Pec-5, (**d**) PVA-Pec-10 and (**e**) PVA-Pec-15 (Scale bar, 1 μm).

2.5. Rheological and mechanical properties investigation

Viscoelastic properties of PVA-Pec hydrogels were evaluated at 37 °C in a Discovery Hybrid Rheometer 3 (TA Instrument, USA) fitted with 20 mm parallel-plate geometry. The test methods employed were oscillatory amplitude sweeps at a constant frequency of 1 Hz. The storage (G') and the loss (G") moduli were recorded while the strain increased from 0.01% to 100%.

The mechanical properties of hydrogels were investigated using a Dynamic Mechanical Analyzer (DMA, MN, USA) at 37 °C. For the tensile test, hydrogels were cut into rectangle shape with length and width of 15 × 3 mm. The initial gauge length was 5 mm and the tests were implemented at the rate of 50% strain per min till sample was broken or reached the maximum length allowed by the equipment (24 mm). Specifically, for cyclic tensile tests, samples were loaded with an initial gauge length of 8 mm before they were extended at a rate of 50% strain per min, to a maximum strain of 100%, followed by slow releasing till returning to their original lengths. Besides, for compressive tests, hydrogels were shaped into cylinders with a diameter of 6 mm and height of 8 mm. Samples were compressed at the rate from −20% to −50% strain per min, followed by −5% strain per min for releasing the samples.

For fatigue experiments, hydrogels samples with a size of 30 mm × 12 mm were prepared. Then they were performed in a water bath at 25 °C with an electronic dynamic and static universal material testing device (Instron, USA). The force used was ranged from 100 to 500 N, the frequency was 4 Hz, and the cycle period was 50,000 times. The axial compression rate was 5 mm/min, and the strain compression was 50%. In order to monitor the real-time state of the specimen in the simulated solution during the compression fatigue experiment, the microcomputer system of the fatigue experiment machine automatically recorded the load displacement time data of the fatigue experiment at each time period, and selected the displacement-time curves of the early and later fatigue periods for analysis.

2.6. Isolation and culture of osteoblasts

Primary osteoblasts were harvested from the parietal bone of newborn Sprague-Dawley (SD) rats (Guangxi Medical University, Nanning, China). Parietal bone slices were digested with 2 mg/ml of collagenase type I (Sigma-Aldrich, USA) for 3 h. The osteoblasts were collected and cultured with Dulbecco's Modified Eagle's Medium (DMEM; Gibco, USA) that containing 10% of (v/v) fetal bovine serum (FBS; Gibco, USA) and 1% of (v/v) penicillin/streptomycin (Solarbio, Beijing, China).

2.7. Cell adhesion

Cells were fixed by 2.5% of glutaraldehyde (Thermo Fisher Scientific, USA) for 0.5 h. Then dehydrated with gradient concentrations of ethanol and further dried by keeping on a clean bench and then observed by XL-30 ESEM-FEG SEM (Hitachi, Japan) after gold coating.

2.8. Cell viability analysis

Osteoblasts were washed three times with PBS, and stained by a Calcein AM/PI stinging kit (Biyotime, Beijing, China) for 5 min in the dark. After washing with PBS, cells were photographed using a fluorescence microscope (Olympus, Japan), and the quantitative analysis was performed with Image J software.

2.9. Cytotoxicity assay

Cells were incubated with 20 μL of MTT at 37 °C for 4 h. The culture medium was replaced with 1 ml of DMSO to dissolve the formazan and the absorption at 570 nm was measured using a Microplate Reader (Thermo Fisher Scientific, USA).

2.10. Quantitative real time polymerase chain reaction (qRT-PCR) analysis

Expression levels of RUNX family transcription factor 2 (*Runx2*), collagen type I alpha 1 chain (*Col1a1*) and alkaline phosphatase (*Alpl*) were investigated by qRT-PCR. The primer sequences used for qRT-PCR were designed as exhibited in Table 1. The RNA was extracted using an RNA isolation kit (Tiangen Biotechnology, Beijing, China) and reversely transcribed into cDNA by a reverse transcription kit (Takara, Japan). qRT-PCR was performed to amplify the cDNA employing the SYBR Premix Ex Tag Kit (ABclonal, Wuhan, China) plus ABI 7500 sequencing detection system (Applied Biosystems, Foster City, CA, USA). Reactions were conducted by a light Cycle 96 system (Roche, Switzerland) under the conditions of 10 min at 95 °C to denature cDNA, then 40 cycles of 10 s at 95 °C and followed by 60 s at 60 °C to hybridize the primer with the target DNA. The glyceraldehyde-3-phosphate dehydrogenase (*Gapdh*) was employed as the internal reference gene. Experiments were carried out in sextuplicate and the comparative $^{2-\Delta\Delta}$Ct method was used for quantification.

2.11. Alkaline Phosphatase (ALP) activity

Cell was collected and lysed with RIPA lysis buffer (Boster, Beijing, China). The supernatant was collected for testing ALP activity using ALP detection reagent kit (Nanjing Jiancheng Bioengineering Research Institute, Nanjing, China). The absorbance at 520 nm was measured using a microplate reader.

2.12. Alizarin Red S staining

Cell were fixed with 4% (w/v) of paraformaldehyde (Biosharp, Wuhan, China) for 0.5 h, and then stained with Alizarin Red S (Solarbio, Beijing, China) for 30 min. The mineralization of osteoblasts was visualized and photographed with a microscope (Olympus, Japan).

Table 1
Primer sequences used in qRT-PCR experiments.

Gene	Forward primer (5'→3')	Forward primer (3'→5')
Runx2	GTGGCCAGGTTCAACGATCT	TGAGGAATGCGCCCTAAATCA
Col1a1	GATCCTGCCGATGTCGCTAT	GGGACTTCTTGAGGTTGCCA
Alpl	GTTACAAGGTGGTGGACGGT	ACAGTGGTCAAGGTTGGCTC
Gapdh	TCCAGTATGACTCTACCCACG	CACGACATACTCAGCACCAG

2.13. Immunofluorescence staining

Cells were fixed with 4% (w/v) of paraformaldehyde for 30 min, followed by incubating with 0.5% (v/v) of Triton X-100 for 15 min. The endogenous peroxidase and nonspecific staining were successively blocked by 3% of hydrogen peroxide and 10% (v/v) of goat serum. Primary antibodies of osteocalcin (OCN; Proteintech, Wuhan, China) and collagen type I (Col1; Proteintech, Wuhan, China) were used and incubated at 4 °C for 12 h. After washed by PBS for 3 times, samples were incubated with second antibody (Boster, Wuhan, China) at 37 °C for 1 h. Subsequently, 2-(4-Amidinophenyl)-6-indolecarbamidine dihydrochloride (DAPI; Beyotime, China) was added for staining the nucleus. Images were obtained by using a confocal laser scanning microscope (CLSM; Leica, Germany).

2.14. Intracellular Ca^{2+} determination

Cells were stained with 4 μM of Fluo-4/AM (Solarbio, Beijing, China) at 37 °C for 25 min, followed by incubating with HBSS (containing 1% FBS) for another 40 min. Subsequently, the cells were washing with N-[2-hydroxyethyl piperazine-N'-[2-ethanesulfonic acid] (HEPES; Solarbio, Beijing, China) buffer and imaged by a fluorescence microscope at a wavelength of 494 nm.

2.15. Western blots (WB)

The protein expression of CaM, p-CaMKII p-SMAD1/5 and BMP-2 were detected by WB analysis according to the previous study [25]. Antibodies against CaM (1:100, Cell Signaling, Technology, America), p-CaMKII Thr286 (1:100, Cell Signaling Technology, America), p-SMAD1/5 (1:100, Cell Signaling, Technology, America) and BMP-2 (1:100, Cell Signaling, Technology, America) were used. GAPDH (1:100, Sangon Biotech, Shanghai, China) was served as the internal protein.

2.16. Animal procedure

A total of forty-five male SD rats weighted of 180–200 g were used. General anesthesia was conducted by injection of pentobarbital (30 mg/kg) intraperitoneally and a defect (3 mm in diameter, 4 mm in depth) was constructed to the distal femur perpendicularly. Then, they were divided into three groups randomly: (1) Control group (without any implanted); (2) PVA group (implanted with PVA); (3) PVA-Pec group (implanted with PVA-Pec-10). After 4 or 8 weeks of therapy, rats were sacrificed to obtain the femurs. All the experiments on animals were approved by the Ethics Committee for Experimental Animals of Guangxi Medical University and performed in accordance with the Chinese national guidelines for the care and use of laboratory animals.

2.17. Micro-CT analysis

The obtained femurs at each time point were scan by a Micro-CT system (Bruker, Germany) with a resolution of 18 μm. Each scan was reconstructed using the same calibration parameters with a source current of 100 mA and a voltage of 100 kV. Bone volume (BV) was calculated to quantify the mineralized tissue at the peripheral zone.

2.18. Histological examination

The femurs were fixed by 4% (w/v) of paraformaldehyde and decalcified with 14% (w/v) of EDTA (MACKLIN, Shanghai, China) under an ultrasonic decalcification machine (MEDITE, Germany). Subsequently, the samples were embedded in paraffin. After cutting into 3 μm slices and dewaxing, hematoxylin and eosin (H&E; Solarbio, Beijing, China) and Masson's trichrome (Solarbio, Beijing, China) staining were performed to evaluate the histological changes.

2.19. Statistical analysis

All data were expressed as the mean ± standard deviation (SD). The statistical analysis was carried out using one-way analysis of variance (ANOVA).

3. Results

3.1. Preparation and characterization of PVA-pec composite hydrogels

The interpenetrated network structure, comprised of the primary semi-crystalline PVA network and the secondary calcium-pectin physical ionic network, formed mechanically robust hydrogels. Not only were the hydrogels capable of withstanding significant deformation without rupture, they were also able to recover to the initial state upon load removal (Fig. 1b).

While the hydrogels appeared to be mechanically robust for bone tissue engineering, their performance were further scrutinized in terms of pore size, network density, water content, degradation and mechanical properties for their potential applications. SEM images showed that all the hydrogels showed porous structures. The pore diameter of PVA-Pec-5 and PVA-Pec-10 hydrogels was relatively close, whereas the PVA-Pec-15 hydrogel exhibited a dense network and the pore diameter significantly decreased (Fig. 1c–e). While PVA-Pec-5 and PVA-Pec-10 hydrogels shared similarity in having large number of macropores, the microstructure of PVA-Pec-10 hydrogel was notably much more ordered and robust than that of PVA-Pec-5 hydrogel.

At water equilibrium state, the hydrogels were found to retain comparable amounts of water in their networks (Fig. 2a, Fig. S1). While the difference was insignificant, it was still noticeable that the water content varied along with the polymer content in the system. Lower water content was observed for the system with higher polymer content. Similarly, the degradation rates of PVA-Pec hydrogels were found to vary with the polymeric density. Compared to the PVA-Pec-5 hydrogel, which lost 44.99 ± 1.29% of mass over 28 days, higher degradation ratios (61.23 ± 1.83% and 68.01 ± 2.09%) were observed for PVA-Pec-10 and PVA-Pec-15 hydrogels (Fig. 2b).

The viscoelastic behavior (storage and loss moduli) of the PVA-Pec hydrogels as a function of oscillation strain was shown in Fig. 2c. Results indicated that the hydrogels were mechanically responsive systems and their rheological properties fluctuated accordingly to the change in stress or strain. At low oscillation strain (<0.1%), linear-viscoelastic (LVE) region was observed with relatively constant storage modulus (G′) and loss modulus (G″). The hydrogel with higher polymer concentration displayed higher G'. As oscillation strain increased, G′ started to decrease, while G″ began to increase, indicating the deformation of the polymer network. After the transition point (G' = G" or Tan δ = 1), the hydrogels changed from solid-like (G' > G″) to liquid-like behavior (G' < G″).

Apart from the viscoelastic behavior, the tensile and compressive properties of the swelled hydrogels were investigated by DMA at body temperature (37 °C). All 3 hydrogels were elastic and tough, and their tensile elongations reached beyond 300% (Fig. 2e). The Young's modulus of the hydrogels increased along with the polymer concentration, which corresponds well with the results obtained for the viscoelastic behavior. The Young's moduli of PVA-Pec-15 reached 117.9 ± 9.0 kPa for tensile test and 79.3 ± 20.6 kPa for compressive test (Fig. 2d and Table S1).

Stress-strain curves of the hydrogels under cyclic loading were shown in Fig. 2f and g. The curves indicated that all the 3 hydrogels were capable of recovering to their original shapes even after 100% extension or 50% compression. The hysteresis loop observed after unloading reveals the viscoelasticity of the material, which occurred possibly due to the breakage of weak but reversible crosslinks under the applied load. As expected, the degree of hysteresis increased with polymer concentration, indicating a larger degree of crosslink dissociation in denser networks. Nevertheless, the results show that all 3 hydrogel compositions possess some degree of energy dissipation and could potentially act as a cushion against external impact. The hydrogels exhibited recovery ability for over 5 cycles where energy dissipation and the occurrence of hysteresis loops were observed (Figs. S2–4). The stress-life behaviors of PVA and PVA-Pec hydrogels are showed in Fig. S5. The fatigue lives of the different hydrogels were revealed to decrease in the order of PVA-Pec-15 > PVA-Pec-10 > PVA-Pec-5> PVA.

3.2. PVA-Pec composite hydrogels improve cell adhesion and viability

The cell adhesion ability was evaluated by SEM. PVA-Pec-10 hydrogels exhibited the best cell adhesion capacity among the three hydrogels (Fig. 2h). As indicated by Calcein-AM/PI staining, less viable cells (green) and more dead cells (red) was present in the PVA group (Fig. 3a and b). Among the three PVA-Pec composite hydrogels, the most live cells and least dead cells were observed in PVA-Pec-10 group. The ratio of live/dead cells in the three PVA-Pec groups was 88.1%, 161.5% and 41.4% higher than the PVA group.

The cytotoxicity was further verified by MTT test. Consistent with the results of the Calcein-AM/PI staining (Fig. 3a–b), the viability of cells cultured on the PVA-Pec composite hydrogels was distinctly increased ($p < 0.001$, Fig. 3c) as compared to the PVA hydrogel. Among the tested samples, PVA-Pec-10 hydrogel showed the highest cell viability with an increase of 57.2% compared to PVA group. The difference between PVA-Pec-5 and PVA-Pec-15 groups was insignificant.

3.3. PVA-Pec composite hydrogels promote osteogensis in vitro

The mRNA levels of osteoblastic markers including *Alpl, Col1a1* and *Runx2* were detected by qRT-PCR analysis. In comparison to PVA hydrogels, the mRNA levels of *Runx2*, *Col1a1* and *Alpl* in osteoblasts cultured on the three PVA-Pec composite hydrogels were distinctly increased (Fig. 4a). In particular, the highest gene expression levels were present in PVA-Pec-10 group, as the level of *Runx2*, *Col1a1* and *Alpl* was 0.4, 1.8 and 9.6-folds higher than the control. There was insignificant difference in the osteogenic gene expression level displayed by PVA-Pec-5 and PVA-Pec-15 hydrogels.

ALP activity is considered a marker that could be used to indicate osteogenesis at the early stage. Compared with the control group, ALP activities were found to be significantly higher for the cells cultured on the PVA-Pec hydrogels ($p < 0.05$, Fig. 4b). While PVA-Pec-5 and PVA-Pec-15 hydrogels brought about improved ALP activities (increase of 93.2% and 211.1% respectively as compared to the PVA hydrogel), the highest ALP activity was exhibited in PVA-Pec-10 hydrogel (a 374.9% increment as compared to PVA hydrogel).

Deposition of mineralized matrix, an important indicator for osteogenic maturation, was stained by Alizarin Red S. Little mineralized ECM was observed in PVA group (Fig. 4c). Among three composite hydrogels, the highest calcium deposition was found in PVA-Pec-10, which was evidenced by the most amounts of nodules deposited on the surface.

The results of immunofluorescence staining of osteogenic protein markers, OCN and Col1, yielded similar results as that of qRT-PCR, ALP activity and Alizarin Red S staining (Fig. 4a–c). Protein expression levels of OCN and Col1 demonstrate that the osteogenic efficiency was much higher in PVA-Pec groups than PVA hydrogel (Fig. 4d). Particularly, positive staining of OCN and Col1 was much obvious for the cells cultured on PVA-Pec-10 hydrogel than those incubated with PVA-Pec-5 or PVA-Pec-15 hydrogels.

3.4. PVA-Pec composite hydrogel enhance osteogenesis via Ca^{2+}/CaMKII and BMP-SMAD1/5 signaling

To explore the osteogenic effect of PVA-Pec-10 hydrogel specifically on Ca^{2+} mediated signaling pathway, the Ca^{2+} influx, CaM and the phosphorylation of its downstream molecule CAMK-II were analyzed. Ca^{2+} influx was significantly elevated in cells cultured on the PVA-Pec-10

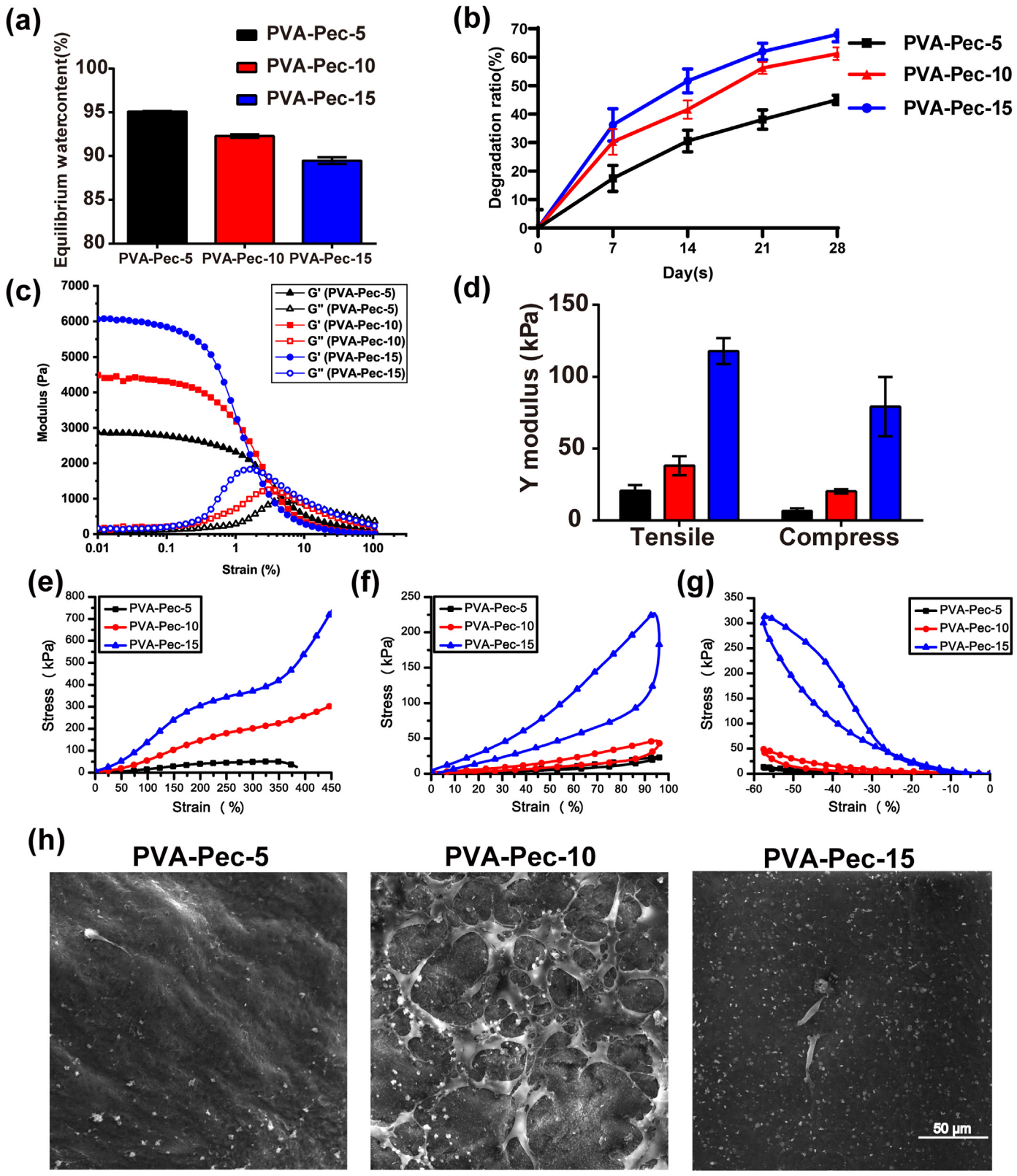

Fig. 2. Mechanical properties and adhesive ability of PVA-Pec composite hydrogels. (a) EWC. (**b**) Degradation behavior. (**c**) Rheology test. (**d**) Young's moduli of hydrogels under tensile and compressive tests. (**e-g**) Stress-strain curves of tensile properties (**e**), cyclic tensile tests (**f**) and cyclic compressive tests (**g**). (**h**) SEM images of osteoblasts cultured on the hydrogels for 7 days (Scale bar, 50 μm).

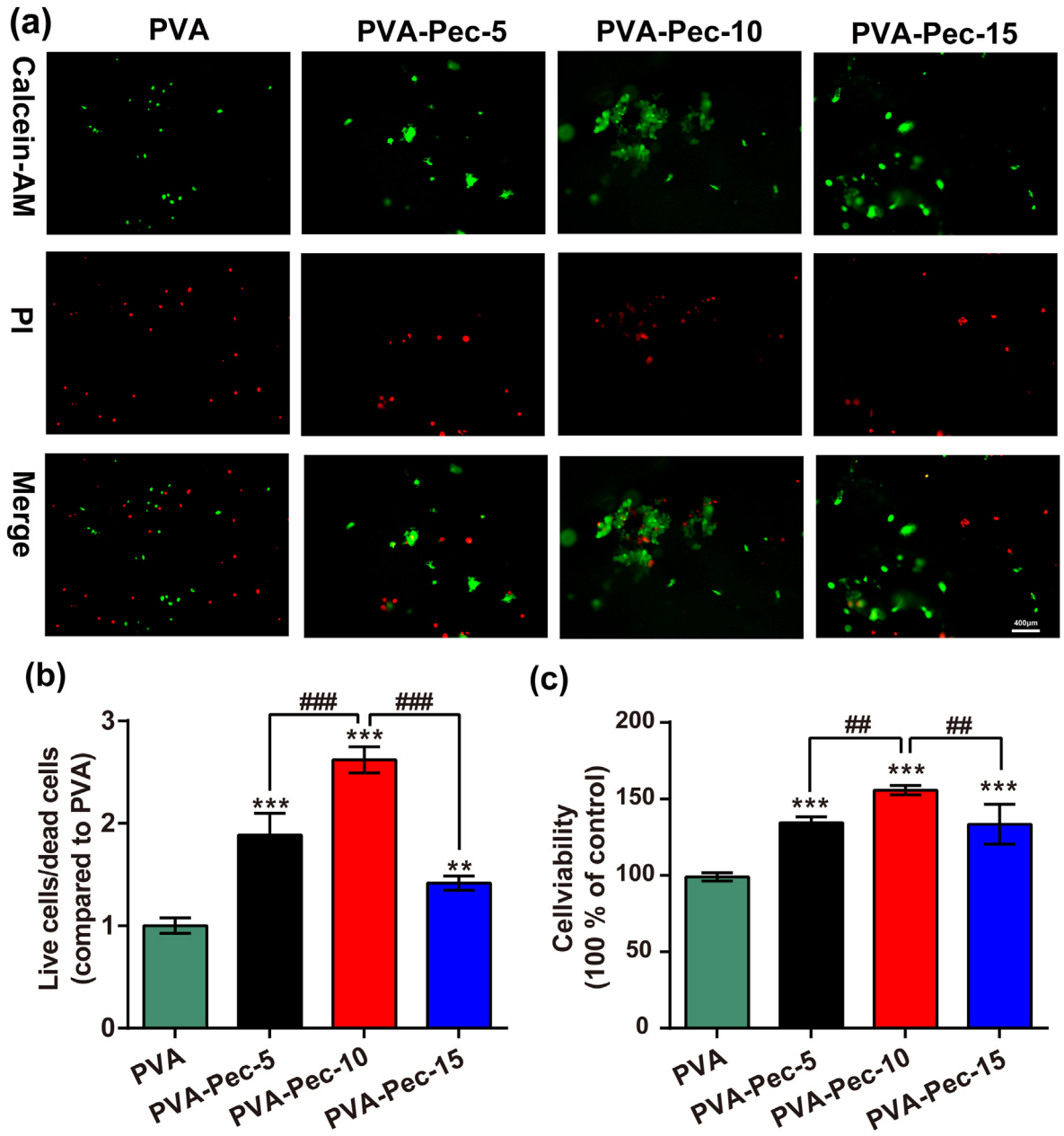

Fig. 3. Viability of osteoblasts cultured on different hydrogels. (**a**) Live/dead cells cultured on hydrogels for 7 d were stained by Calcein AM/PI (Scale bar, 400 μm). (**b**) Quantification of the ratio of live and dead cells in (**a**). (**c**) Viability of cells cultured on hydrogels for 7 d was detected by MTT assay (Mean ± SD, n = 3; **, ## mean $p < 0.01$, ***, ### mean $p < 0.001$).

(Fig. 5a). Similarly, the expression of CaM and CAMK-II phosphorylation substantially enhanced in the cells cultured on the PVA-Pec-10 hydrogel compared to PVA and pectin (Fig. 5b and c). Given the significance of the BMP-SMAD 1/5 signaling in the osteogenesis, the expression of BMP-2 and p-SMAD1/5 was also examined. It revealed that higher expression level of BMP-2 was detected in the PVA-Pec-10 group, while lower levels were seen in the PVA and pectin group (Fig. 5d). A similar trend was identified for the expression of p-SMAD1/5 (Fig. 5e).

3.5. PVA-Pec composite hydrogels accelerate femur regeneration in vivo

Micro-CT was used to evaluate the repair of femoral defects in SD mice. At week 4, bone defects were still unrepaired in the control group (Fig. 6a–b). In contrast, implantation of PVA or PVA-Pec hydrogels achieved visible new bone formation. At 8 weeks post-operation, the defect was still clearly observed in the control group. Although the defect still remained for the PVA group, there was large amount of newly formed tissue that successfully bridged the defect in PVA group. The 8 weeks implantation of PVA-Pec hydrogels showed even better results with the regions of defects well integrated to the host bone. Further morphometry analysis of the region of defects demonstrated that the BV of control group was significantly lower than that of PVA-Pec hydrogel at week 4 ($p < 0.05$) (Fig. 6c–d). The difference between PVA and PVA-Pec hydrogels was insignificant. At week 8, the BV of PVA-Pec group had emerged distinctly higher than control and PVA groups (increase of 53.0% and 52.5%).

H&E staining shows that macroscopic observation demonstrated that bone defects were still unrepaired in the control group and the implantation of PVA-Pec achieved successful bridging with bony union on weeks 4 of therapy (Fig. 7a). In control group, even though large amount of newly formed tissue successfully bridged the defect at 8 weeks post operation, there was a clear boundary between the new tissue and the

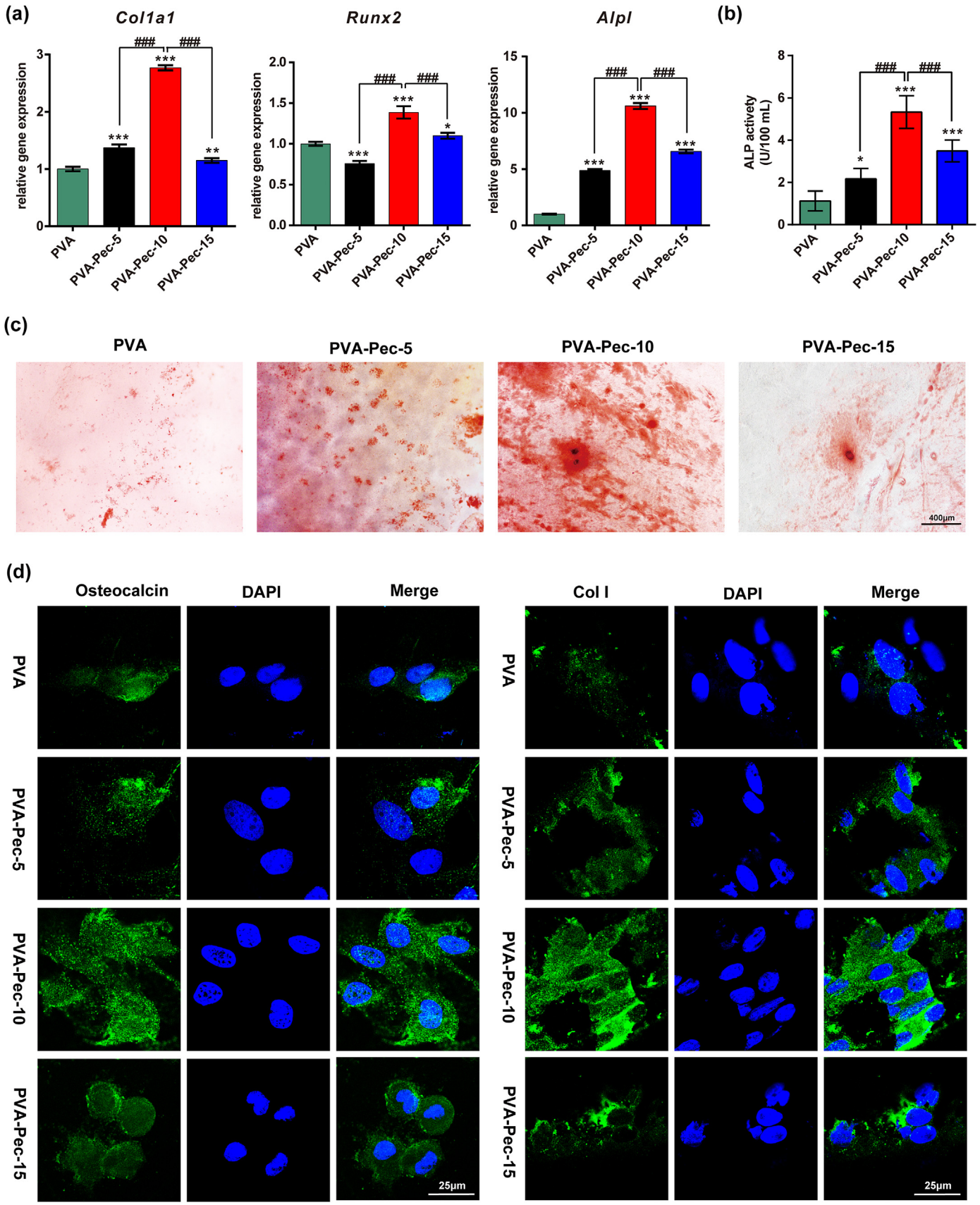

Fig. 4. Osteogenesis effect of PVA-Pec hydrogels *in vitro*. (**a**) The gene expression levels of *Runx2, Col1a1* and *Alpl*. (**b**) ALP activity. (**c**) ARS staining (Scale bar, 400 μm). (**d**) Immunofluorescence staining for OCN and Col1 (Scale bar, 25 μm. Mean ± SD, n = 3; * means $p < 0.05$, ** means $p < 0.01$, ***, $^{###}$ mean $p < 0.001$).

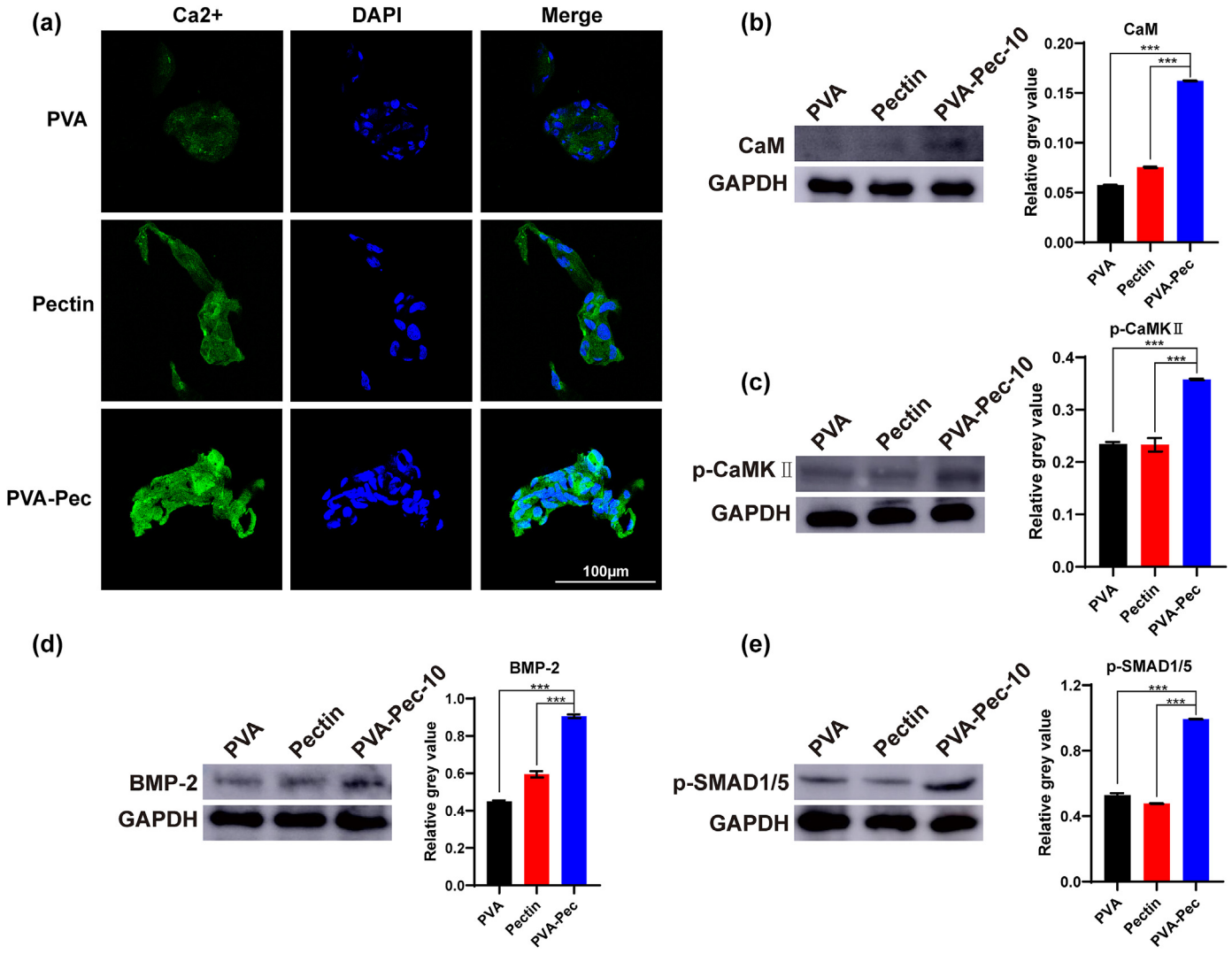

Fig. 5. PVA-Pec composite hydrogel accelerates the process of osteogenesis by mediating Ca^{2+}/CaMKII and BMP-SMAD1/5 signaling. (**a**) Ca^{2+} influx in osteoblasts cultured on the PVA, pectin or PVA-Pec-10 hydrogels were analyzed by fluo-4/AM probe (Scale bar, 100 μm). (**b-e**) The levels of CaM (**b**), p-CaMKII (**c**) p-SMAD1/5 (**d**) and BMP-2 (**e**) in osteoblasts cultured on the PVA, pectin or PVA-Pec-10 hydrogels were detected by WB (Mean ± SD, n = 3; *** means $p < 0.001$).

host tissue. By implantation of PVA-Pec hydrogel for 8 weeks, the newly formed tissue showed well integration to the host tissues and exhibited high similarity to the native bone tissue.

The assessment of bone restoration was additionally evaluated by Masson's trichrome staining. Clear defects were still present in the control group after 4 weeks of therapy and the defects were filled with connective fibrous tissue with limited new bone tissue formation (Fig. 7b). In contrast, PVA-Pec hydrogels were integrated with the native bone tissue at week 4 and the successful defect healing was observed at week 8.

4. Discussion

Composite hydrogels consist of interpenetrating networks which act cooperatively to endow hydrogels with good mechanical property are reported to be conducive for bone regeneration [6,12]. In this study, we developed physical crosslinked composite hydrogels to support and even accelerate the bone regeneration process. The composite hydrogels were established based on the hydrogen bonding between PVA, the ionic interaction between Ca^{2+} and pectin, and the interaction force between PVA and pectin (Fig. S6). An advantage of this hydrogel system is the evasion of any potential toxicity issue, that tends to exist for chemically crosslinking system.

Since bone is a hard tissue in human body, it is necessary to improve the mechanical properties of the hydrogels to achieve suitable stiffness for bone tissue engineering [26]. Our results showed that an increase in polymer concentration contributed to the increase in the density of polymeric network. This could possibly be accounted for the improvement in the mechanical properties of the composite hydrogels given that more bonds are present. Through adjusting the concentration of polymer to 15%, the composite hydrogel achieved high tensile strength of 117.9 ± 9.0 kPa and compressive strength of 79.3 ± 20.6 kPa. Higher polymer concentration also resulted in higher porosity (Fig. 1c–e) but lower swelling ratio (Fig. S1), water content (Fig. 2a) and weight loss (Fig. 2b). In addition, the favorable resilience ability which is dependent on the polymeric structure of hydrogel and its homogeneous distribution of polymers is of significance for bone healing. During the compression, no fracture was observed in the PVA-Pec hydrogels which indicates that improvement in the mechanical properties was achieved. Furthermore, the recovery of the PVA-Pec hydrogel to its original shape after the applied load was removed suggests that the developed hydrogel possessed shape memory property (Fig. 1b). The ability to withstand repeated loading is suitable for bone tissue engineering, where repeated loadings are expected given that bones serve the load bearing function.

Adhesion is an important regulator in cell differentiation, migration and proliferation [27]. PVA hydrogels were reported with non-ideal protein adsorption and cell adhesion due to the lack of cell affiliation

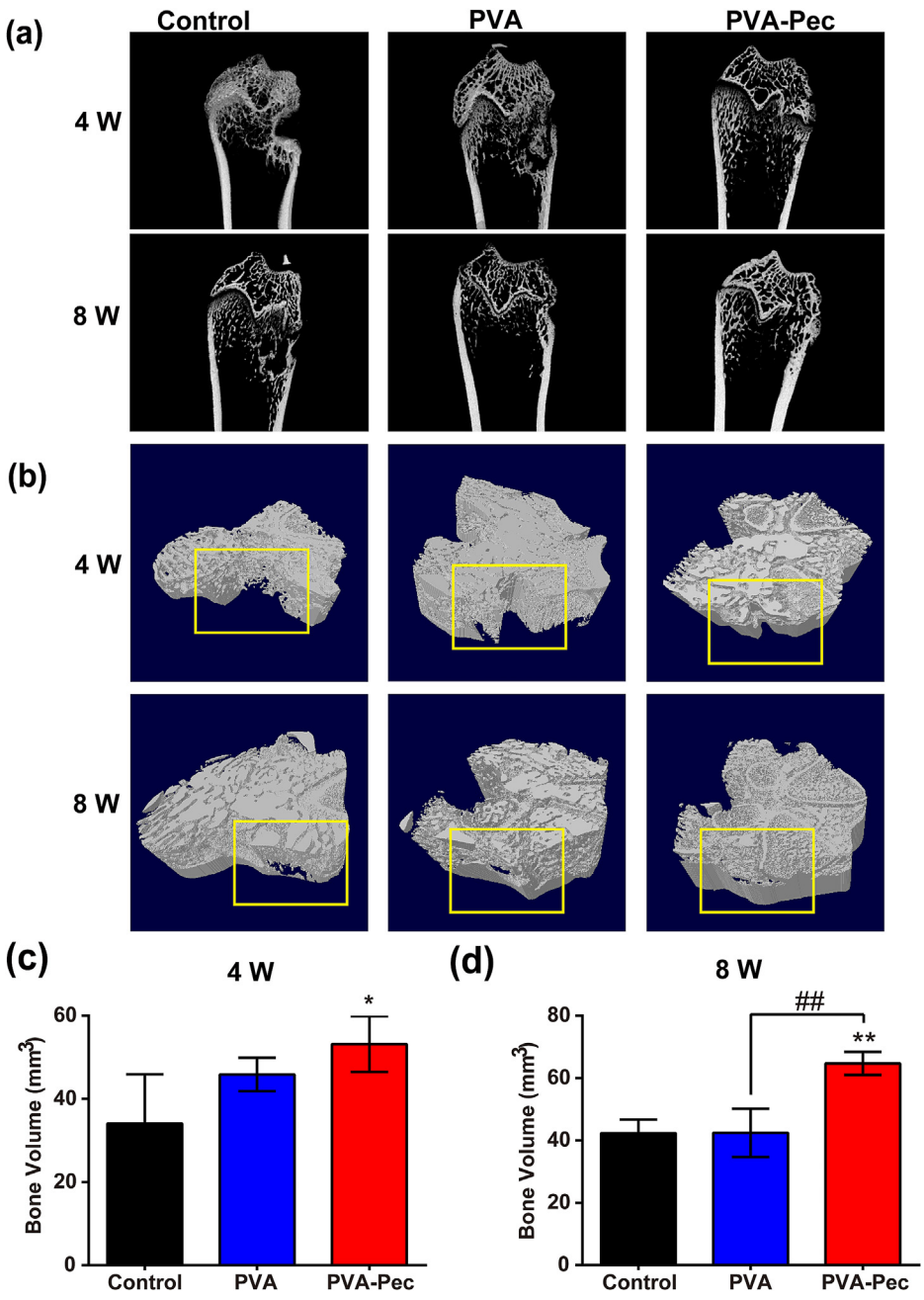

Fig. 6. Micro-CT analysis of the hydrogel implanted defects. (**a-b**) Representative microcomputed tomography images of joints for (**a**) sagittal section and (**b**) axial section at week 4 and 8 post-treatment. (**c-d**) BV as measured by Micro-CT. (Mean ± SD, n = 3; * means $p < 0.05$, **, ## mean $p < 0.01$).

groups on its surface [28]. On the other hand, as a biomolecule, pectin contains large number of functional groups that are capable of binding to cell receptors to induce cell adhesion [29]. The formation of "egg-box structure" in pectin-based hydrogels is also beneficial for the cell adhesion as it allows cell immobilization. Lin et al. engineered pectin/chitosan hydrogels with improved mechanical properties and biocompatibility which showed the best biocompatibility and capacity of mineralization with osteoblast cells [30]. Moreover, pectin gel was used as a carrier for the stem cells to facilitate bone in-growth because of its low immunogenicity [31]. In our results, PVA-Pec-10 hydrogel showed favorable adhesion properties as compared to PVA-Pec-5 and PVA-Pec-15 hydrogels, probably due to its balance of stiffness and scaffold pore size (Fig. 2h). It was reported that the matrix elasticity plays a role in guiding the cell differentiation. Within the range of 25–40 kPa, the matrix was found to lead to osteoblast development from mesenchymal stem cells [32]. PVA-Pec-10 demonstrated a suitable stiffness (with compressive Young's modulus of 20.3 ± 1.5 kPa and tensile Young's modulus of 38.1 ± 6.5 kPa) for the osteoblast development whereas the stiffness of PVA-Pec-5 and PVA-Pec-15 were not as close and even out of the reported range. It was not surprising that highest viability of osteoblasts was observed for the PVA-Pec-10 (Fig. 3).

Mineralization of the matrix is a key factor to trigger cytodifferentiation of osteoblasts from a plump immature form to a mature cell [33]. As evidenced by Alizarin Red S staining, matrix mineralization of osteoblast was accelerated when seeded in PVA-Pec hydrogels compared to PVA (Fig. 4c). ALP, an initial marker for osteoblasts that have entered the extracellular matrix maturity stage [34], was significantly higher in PVA-Pec hydrogels than in PVA hydrogels (Fig. 4b). The expression levels of osteogenic specific genes (*Alpl*, *Col1a1* and *Runx2*) in osteoblasts cultured on the PVA-Pec hydrogels coincided with the results of ALP

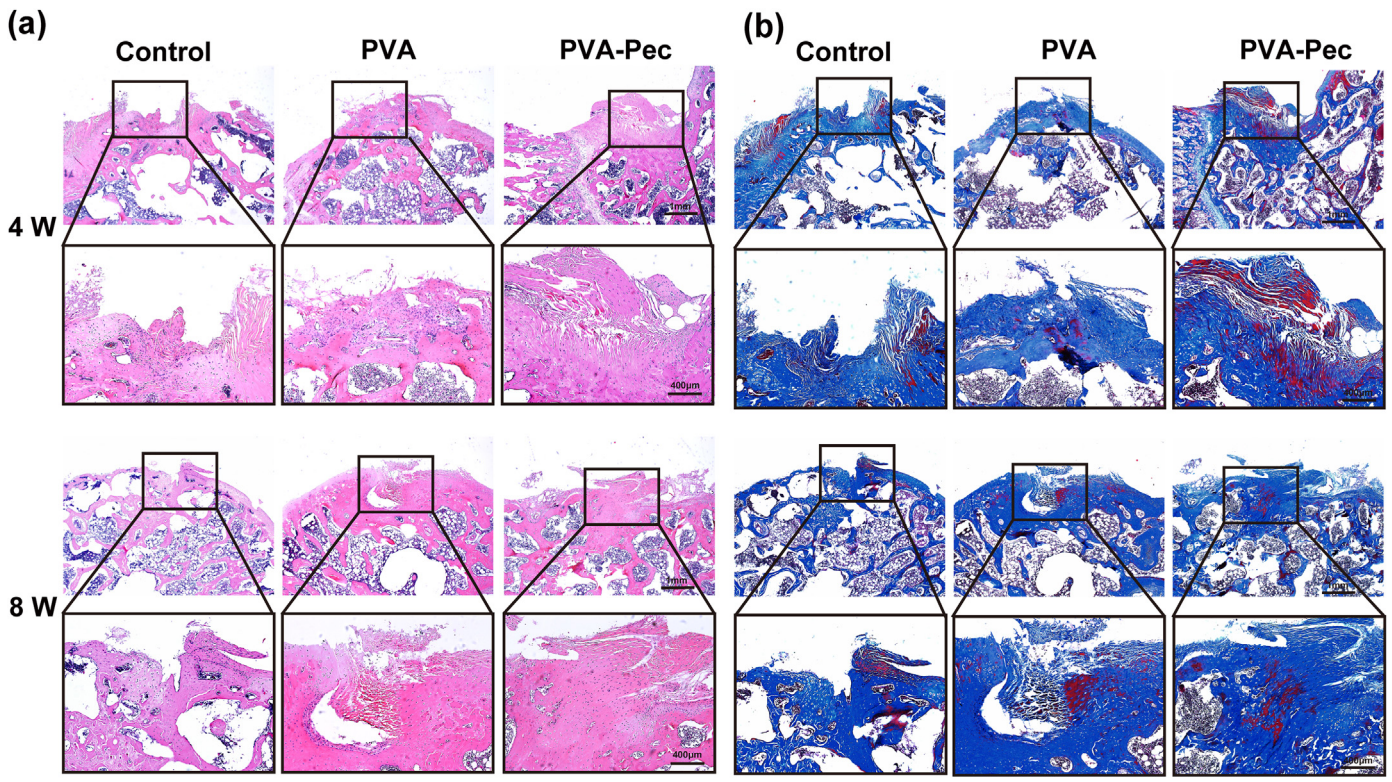

Fig. 7. Histological evaluation of bone defects that repaired by implanting hydrogels. (**a**) H&E staining was performed to observe the morphology. (**b**) Masson's trichrome staining was performed to assess the new bone formation (Scale bars = 1mm or 400 μm).

activity (Fig. 4a). OCN, hydroxyapatite-binding noncollagenous ECM proteins secreted by osteoblast, represents the phenotype of mature osteoblast [35]. Col1, a protein abundantly found in the bone extracellular matrix, is essential for bone strength [36]. As evidenced by the immunofluorescence staining for OCN and Col1, PVA-Pec-10 hydrogel stimulated higher expression of both proteins (Fig. 4d). PVA-Pec-10 hydrogel was implanted into the bone defects of rats *in vivo* to verify the impact of PVA-Pec on bone restoration. The bone healing process was found to be accelerated by the implantation of PVA-Pec-10 hydrogel (Figs. 6 and 7).

Mechanotransduction plays an essential role in osteogenesis. The crosstalk between mechanotransduction pathways and BMP-2 signaling is due to the phosphorylation of receptor-activated Smad1/5 [23]. The activated SMADs then form a SMAD complex that translocates to the cell nucleus and regulates the osteogenic gene expression. PVA-Pec-10 hydrogel enhanced the expression of BMP-2 and SMAD1/5 as compared to PVA and pectin hydrogels, suggesting that the improvement of stiffness promotes osteogenesis through regulating the BMP-SMAD1/5 signaling (Fig. 5d–e).

A further notable characteristic of the PVA-Pec composite hydrogels, enriched with polymer-Ca^{2+}-complex, is their capacity to enhance the mineralization of osteoblast. Calcium has been well established to affect the cellular proliferation, differentiation and function via modulating the transcriptional change in gene expression [37]. In the study, we demonstrated that the Ca^{2+}/CaMKII signaling is involved in the osteogenesis of osteoblasts cultured on the PVA-Pec hydrogel (Fig. 5). CaM is the E–F-hand family of Ca^{2+}-sensing proteins, expresses in all eukaryotic cells where it participates in signaling pathways that regulate many crucial processes such as growth, proliferation and movement [38]. When bound with CaM (a small Ca^{2+}-binding protein) [39], a Ca^{2+}/CaM complex forms that can phosphorylate and activate CaM-dependent kinase II (CaMK-II) to affect the functions of osteoblasts [40,41]. In a separate study, Shin et al. revealed that Ca^{2+}/CaMKII/ERK/AP-1 signaling pathway is crucial in the process of osteogenic differentiation of stem cells induced by collagen-binding peptide [37]. Bagne et al. also demonstrated that an increase in cytosolic Ca^{2+} and the activation of CaM brought about by the allogeneic graft or bioactive glass could further favor bone repair [42].

5. Conclusions

The composite hydrogels formed by physical crosslinking of PVA and pectin were successfully fabricated for bone tissue engineering. The produced composite hydrogels possess suitable mechanical properties, high porosity, decent bioactivity and osteoconductive capability. The addition of Ca^{2+} for the formation of PVA-Pec composite hydrogels also contributed to accelerate mineralization of the matrix. Owing to the appropriate mechanical properties and excellent adhesion ability, PVA-Pec-10 hydrogel greatly stimulated the matrix mineralization *in vitro* and accelerated the bone healing *in vivo* via regulating Ca^{2+}/CaMKII and BMP-SMAD1/5 signaling. The PVA-Pec hydrogels show promise as the regenerative materials for bone tissue engineering.

Credit authorstatement

Ziwei Hu: Visualization, Investigation, Data curation. **Jianwen Cheng**: Resources, Writing – review & editing. **Sheng Xu**: Investigation, Data curation. **Xiaojing Cheng**: Data curation. **Zhi Wei Kenny Low**: Data curation. **Pei Lin Chee:** Data curation. **Zhenhui Lu**: Resources, Writing – review & editing. **Li Zheng**: Visualization, Investigation, Writing – original draft. **Dan Kai**: Resources, Writing – review & editing. **Jinmin Zhao**: Resources, Writing – review & editing.

Declaration of competing interest

The authors declare that they have no known competing financial interests or personal relationships that could have appeared to influence the work reported in this paper.

Acknowledgments

This study was financially supported by the Guangxi Science, Technology Base and Talent Special Project (Grant No. GuikeAD19254003), the Guangxi Science and Technology Major Project (Grant No. GuikeAA19254002) and China Postdoctoral Science Foundation (2021MD703815). The authors gratefully acknowledge the financial support from the Agency of Science, Technology and Research (A*STAR).

Appendix A. Supplementary data

Supplementary data to this article can be found online at https://doi.org/10.1016/j.mtbio.2022.100431.

References

[1] A. Noori, S.J. Ashrafi, R. Vaez-Ghaemi, A. Hatamian-Zaremi, T.J. Webster, A review of fibrin and fibrin composites for bone tissue engineering, Int. J. Nanomed. 12 (2017) 4937–4961, https://doi.org/10.2147/ijn.S124671.

[2] M.P. Prabhakaran, J. Venugopal, S. Ramakrishna, Electrospun nanostructured scaffolds for bone tissue engineering, Acta Biomater. 5 (2009) 2884–2893, https://doi.org/10.1016/j.actbio.2009.05.007.

[3] C. Zhao, N.T. Qazvini, M. Sadati, Z. Zeng, S. Huang, A.L. De La Lastra, L. Zhang, Y. Feng, W. Liu, B. Huang, B. Zhang, Z. Dai, Y. Shen, X. Wang, W. Luo, B. Liu, Y. Lei, Z. Ye, L. Zhao, D. Cao, L. Yang, X. Chen, A. Athiviraham, M.J. Lee, J.M. Wolf, R.R. Reid, M. Tirrell, W. Huang, J.J. de Pablo, T.C. He, A pH-triggered, self-assembled, and bioprintable hybrid hydrogel scaffold for mesenchymal stem cell based bone tissue engineering, ACS Appl. Mater. Interfaces 11 (2019) 8749–8762, https://doi.org/10.1021/acsami.8b19094.

[4] S. Stratton, N.B. Shelke, K. Hoshino, S. Rudraiah, S.G. Kumbar, Bioactive polymeric scaffolds for tissue engineering, Bioact. Mater. 1 (2016) 93–108, https://doi.org/10.1016/j.bioactmat.2016.11.001.

[5] M. M, T. A, P. Cp, T. S, A. A, N. M, A. D.-P, Nanoreinforced hydrogels for tissue engineering: biomaterials that are compatible with load-bearing and electroactive tissues, Adv. Mater. 29 (2017), 1603612, https://doi.org/10.1002/adma.201603612.

[6] T. Nonoyama, S. Wada, R. Kiyama, N. Kitamura, M.T. Mredha, X. Zhang, T. Kurokawa, T. Nakajima, Y. Takagi, K. Yasuda, J.P. Gong, Double-network hydrogels strongly bondable to bones by spontaneous osteogenesis penetration, Adv. Mater. 28 (2016) 6740–6745, https://doi.org/10.1002/adma.201601030.

[7] M. Laurenti, A. Al Subaie, M.N. Abdallah, A.R. Cortes, J.L. Ackerman, H. Vali, K. Basu, Y.L. Zhang, M. Murshed, S. Strandman, J. Zhu, N. Makhoul, J.E. Barralet, F. Tamimi, Two-dimensional magnesium phosphate nanosheets form highly thixotropic gels that up-regulate bone formation, Nano Lett. 16 (2016) 4779–4787, https://doi.org/10.1021/acs.nanolett.6b00636.

[8] J.P. Gong, Y. Katsuyama, T. Kurokawa, Y. Osada, Double network hydrogels with extremely high mechanical strength, Adv. Mater. 15 (2010) 1155–1158, https://doi.org/10.1002/adma.200304907.

[9] X.-H. Wang, F. Song, D. Qian, Y.-D. He, W.-C. Nie, X.-L. Wang, Y.-Z. Wang, Strong and tough fully physically crosslinked double network hydrogels with tunable mechanics and high self-healing performance, Chem. Eng. J. 349 (2018) 588–594, https://doi.org/10.1016/j.cej.2018.05.081.

[10] J. Chen, J. Huang, Y. Hu, 3D printing of biocompatible shape-memory double network hydrogels, ACS Appl. Mater. Interfaces 13 (2021) 12726–12734, https://doi.org/10.1021/acsami.0c17622.

[11] J. Zhang, L. Chen, B. Shen, L. Chen, J. Feng, Ultra-high strength poly(N-(2-hydroxyethyl)acrylamide)/chitosan hydrogel with "repelling and killing" bacteria property, Carbohydr. Polym. 225 (2019), 115160, https://doi.org/10.1016/j.carbpol.2019.115160.

[12] M.T.I. Mredha, N. Kitamura, T. Nonoyama, S. Wada, K. Goto, X. Zhang, T. Nakajima, T. Kurokawa, Y. Takagi, K. Yasuda, J.P. Gong, Anisotropic tough double network hydrogel from fish collagen and its spontaneous in vivo bonding to bone, Biomaterials 132 (2017) 85–95, https://doi.org/10.1016/j.biomaterials.2017.04.005.

[13] M.F.A. Cutiongco, S.H. Goh, R. Aid-Launais, C.L. Visage, Y.L. Hong, E.K.F. Yim, Planar and tubular patterning of micro and nano-topographies on poly(vinyl alcohol) hydrogel for improved endothelial cell responses, Biomaterials 84 (2016) 184–195, https://doi.org/10.1016/j.biomaterials.2016.01.036.

[14] G. Francius, J. Hemmerlé, J. Ohayon, P. Schaaf, J.C. Voegel, C. Picart, B. Senger, Effect of crosslinking on the elasticity of polyelectrolyte multilayer films measured by colloidal probe AFM, Microsc. Res. Tech. 69 (2006) 84–92, https://doi.org/10.1002/jemt.20275.

[15] H.R. Moreira, F. Munarin, R. Gentilini, L. Visai, P.L. Granja, M.C. Tanzi, P. Petrini, Injectable pectin hydrogels produced by internal gelation: pH dependence of gelling and rheological properties, Carbohydr. Polym. 103 (2014) 339–347, https://doi.org/10.1016/j.carbpol.2013.12.057.

[16] N. Ninan, M. Muthiah, I.-K. Park, A. Elain, S. Thomas, Y. Grohens, Pectin/carboxymethyl cellulose/microfibrillated cellulose composite scaffolds for tissue engineering, Carbohydr. Polym. 98 (2013) 877–885, https://doi.org/10.1016/j.carbpol.2013.06.067.

[17] R.F. Pereira, C.C. Barrias, P.J. Bártolo, P.L. Granja, Cell-instructive pectin hydrogels crosslinked via thiol-norbornene photo-click chemistry for skin tissue engineering, Acta Biomater. 66 (2017), https://doi.org/10.1016/j.actbio.2017.11.016. S1742706117307006.

[18] F. Munarin, S.G. Guerreiro, M.A. Grellier, M.C. Tanzi, P.L. Granja, Pectin-based injectable biomaterials for bone tissue engineering, Biomacromolecules 12 (2011) 568–577, https://doi.org/10.1021/bm101110x.

[19] M. Shinichi, N. Yasuo, M. Hideo, M. Hideo, Y. Taku, F. Atsushi, T. Yoshiaki, T. Tetsushi, T. Junzo, The effect of calcium ion concentration on osteoblast viability, proliferation and differentiation in monolayer and 3D culture, Biomaterials 26 (2005) 4847–4855, https://doi.org/10.1016/j.biomaterials.2005.01.006.

[20] M. Zayzafoon, Calcium/calmodulin signaling controls osteoblast growth and differentiation, J. Cell. Biochem. 97 (2006) 56–70, https://doi.org/10.1002/jcb.20675.

[21] J. Li, C. Liu, Y. Li, Q. Zheng, Y. Xu, B. Liu, W. Sun, Y. Li, S. Ji, M. Liu, J. Zhang, D. Zhao, R. Du, Z. Liu, G. Zhong, C. Sun, Y. Wang, J. Song, S. Zhang, J. Qin, S. Ling, X. Wang, Y. Li, TMCO1-mediated Ca(2+) leak underlies osteoblast functions via CaMKII signaling, Nat. Commun. 10 (2019) 1589, https://doi.org/10.1038/s41467-019-09653-5.

[22] M. Zayzafoon, K. Fulzele, J.M. McDonald, Calmodulin and calmodulin-dependent kinase IIalpha regulate osteoblast differentiation by controlling c-fos expression, J. Biol. Chem. 280 (2005) 7049–7059, https://doi.org/10.1074/jbc.M412680200.

[23] Q. Wei, A. Holle, J. Li, F. Posa, F. Biagioni, O. Croci, A.S. Benk, J. Young, F. Noureddine, J. Deng, M. Zhang, G.J. Inman, J.P. Spatz, S. Campaner, E.A. Cavalcanti-Adam, BMP-2 signaling and mechanotransduction synergize to drive osteogenic differentiation via YAP/TAZ, Adv. Sci. 7 (2020), 1902931, https://doi.org/10.1002/advs.201902931.

[24] F. Munarin, S.G. Guerreiro, M.A. Grellier, M.C. Tanzi, M.A. Barbosa, P. Petrini, P.L. Granja, Pectin-based injectable biomaterials for bone tissue engineering, Biomacromolecules 12 (2011) 568–577, https://doi.org/10.1021/bm101110x.

[25] T. Jiang, D. Kai, S. Liu, X. Huang, S. Heng, J. Zhao, B.Q.Y. Chan, X.J. Loh, Y. Zhu, C. Mao, L. Zheng, Mechanically cartilage-mimicking poly(PCL-PTHF urethane)/collagen nanofibers induce chondrogenesis by blocking NF-kappa B signaling pathway, Biomaterials 178 (2018) 281–292, https://doi.org/10.1016/j.biomaterials.2018.06.023.

[26] Y. Zhao, Z. Cui, B. Liu, J. Xiang, D. Qiu, Y. Tian, X. Qu, Z. Yang, An injectable strong hydrogel for bone reconstruction, Adv. Healthc. Mater. 8 (2019), e1900709, https://doi.org/10.1002/adhm.201900709.

[27] D.E. Pegg, Principles of tissue engineering, Cryobiology 39 (2000) 378–379, https://doi.org/10.1006/cryo.1999.2214.

[28] R.H. Schmedlen, K.S. Masters, J.L. West, Photocrosslinkable polyvinyl alcohol hydrogels that can be modified with cell adhesion peptides for use in tissue engineering, Biomaterials 23 (2002) 4325–4332, https://doi.org/10.1016/s0142-9612(02)00177-1.

[29] L.S. Liu, Y.J. Won, P.H. Cooke, D.R. Coffin, M.L. Fishman, K.B. Hicks, P.X. Ma, Pectin/poly(lactide-co-glycolide) composite matrices for biomedical applications, Biomaterials 25 (2004) 3201–3210, https://doi.org/10.1016/j.biomaterials.2003.10.036.

[30] I.H. Liu, S.H. Chang, H.Y. Lin, Chitosan-based hydrogel tissue scaffolds made by 3D plotting promotes osteoblast proliferation and mineralization, Biomed. Mater. 10 (2015), 035004, https://doi.org/10.1088/1748-6041/10/3/035004.

[31] M. Tschon, S. Brogini, A. Parrilli, S. Bertoldi, A. Silini, O. Parolini, S. Faré, L. Martini, F. Veronesi, M. Fini, G. Giavaresi, Assessment of the in vivo biofunctionality of a biomimetic hybrid scaffold for osteochondral tissue regeneration, Biotechnol. Bioeng. 118 (2021) 465–480, https://doi.org/10.1002/bit.27584.

[32] A.J. Engler, S. Sen, H.L. Sweeney, D.E. Discher, Matrix elasticity directs stem cell lineage specification, Cell 126 (2006) 677–689, https://doi.org/10.1016/j.cell.2006.06.044.

[33] K. Irie, S. Ejiri, Y. Sakakura, T. Shibui, T. Yajima, Matrix mineralization as a trigger for osteocyte maturation, J. Histochem. Cytochem. 56 (2008) 561–567, https://doi.org/10.1369/jhc.2008.950527.

[34] L. Hao, L. Li, P. Wang, Z. Wang, X. Shi, M. Guo, P. Zhang, Synergistic osteogenesis promoted by magnetically actuated nano-mechanical stimuli, Nanoscale 11 (2019) 23423–23437, https://doi.org/10.1039/c9nr07170a.

[35] J.R. Porter, A. Henson, K.C. Popat, Biodegradable poly(epsilon-caprolactone) nanowires for bone tissue engineering applications, Biomaterials 30 (2009) 780–788, https://doi.org/10.1016/j.biomaterials.2008.10.022.

[36] K.S. Tsai, S.Y. Kao, C.Y. Wang, Y.J. Wang, J.P. Wang, S.C. Hung, Type I collagen promotes proliferation and osteogenesis of human mesenchymal stem cells via activation of ERK and Akt pathways, J. Biomed. Mater. Res. A. 94 (2010) 673–682, https://doi.org/10.1002/jbm.a.32693.

[37] M.K. Shin, M.K. Kim, Y.S. Bae, I. Jo, S.J. Lee, C.P. Chung, Y.J. Park, S. Min do, A novel collagen-binding peptide promotes osteogenic differentiation via Ca2+/calmodulin-dependent protein kinase II/ERK/AP-1 signaling pathway in human bone marrow-derived mesenchymal stem cells, Cell. Signal. 20 (2008) 613–624, https://doi.org/10.1016/j.cellsig.2007.11.012.

[38] D. Chin, A.R. Means, Calmodulin: a prototypical calcium sensor, Trends Cell Biol. 10 (2000) 322–328, https://doi.org/10.1016/s0962-8924(00)01800-6.

[39] M. Zayzafoon, Calcium/calmodulin signaling controls osteoblast growth and differentiation, J. Cell. Biochem. 97 (2006) 56–70, https://doi.org/10.1002/jcb.20675.

[40] J. Li, C. Liu, Y. Li, Q. Zheng, Y. Xu, B. Liu, W. Sun, Y. Li, S. Ji, M. Liu, J. Zhang, D. Zhao, R. Du, Z. Liu, G. Zhong, C. Sun, Y. Wang, J. Song, S. Zhang, J. Qin, S. Ling, X. Wang, Y. Li, TMCO1-mediated Ca(2+) leak underlies osteoblast functions via

CaMKII signaling, Nat. Commun. 10 (2019) 1589, https://doi.org/10.1038/s41467-019-09653-5.

[41] M. Zayzafoon, K. Fulzele, J.M. McDonald, Calmodulin and calmodulin-dependent kinase IIalpha regulate osteoblast differentiation by controlling c-fos expression, J. Biol. Chem. 280 (2005) 7049–7059, https://doi.org/10.1074/jbc.M412680200.

[42] L. Bagne, M.A. Oliveira, A.T. Pereira, G.F. Caetano, C.A. Oliveira, A.A. Aro, G.B. Chiarotto, G.M.T. Santos, F.A.S. Mendonça, M. Santamaria Jr., Electrical therapies act on the Ca(2+)/CaM signaling pathway to enhance bone regeneration with bioactive glass [S53P4] and allogeneic grafts, J. Biomed. Mater. Res. B Appl. Biomater. 109 (2021) 2104–2116, https://doi.org/10.1002/jbm.b.34858.